AAS 96-047

Techniques for Real-Time Control of Flexible Structures Using GPS

E. Harrison Teague*, Jonathan P. How†, London G. Lawson‡,
Michael Boerjes§, Bradford W. Parkinson¶

Department of Aeronautics and Astronautics, Stanford University, Stanford CA

ABSTRACT

This paper describes the most recent advances in our research on GPS (global positioning system) for real-time structural motion sensing and control. The goal of this work is to bring to light the important issues that arise when expanding GPS to deformation sensing, to find and show solutions to these issues, and to demonstrate this technology experimentally. We have shown 20 Hz differential carrier phase measurements with ~ 5 mm relative position accuracy on a test structure which emulates the dynamic motions of a flexible orbiting structure. The GPS receivers provide measurements from an array of antennas mounted on the test structure. Simultaneous measurements from rate-gyro sensors are used for comparison and verification.

In this paper, we discuss and quantify errors which are encountered when using signals from pseudolites (GPS-like signal generators) whose wavefronts are not well approximated as planar, and we explore, in general, the use of multiple receiver, multiple antenna sensor arrays. The corresponding impact of these topics on our experiment is discussed. Also, details of the test structure and current data are presented and analyzed.

1 Introduction

Direct position sensing systems rely on the measurement of a signal or field which is "fixed" or originates from a fixed source. A sensor must be in the domain of influence of this source, and is thus useful in a limited area. Typically, there has been a trade-off between domain of influence and measurement accuracy. For example, high accuracy laser and microwave sensors have small domains, while coarse gravitometers and magnetometers have large domains, in a relative sense. Loran is in between. Inertial sensors attempt to provide location independent position information, but are encumbered by errors which grow with time. The value of GPS positioning lies in the combination of its extensive domain and high accuracy. The same GPS signal has been shown to provide position information to land, sea, air and space vehicles with essentially the same accuracy.

* Graduate research assistant, PhD. candidate, Dept. Aeronautics and Astronautics
† Assistant professor, Dept. Aeronautics and Astronautics
‡ Graduate research assistant, MS candidate, Dept. Aeronautics and Astronautics
§ Research assistant, Junior, Dept. Electrical Engineering
¶ Professor, Dept. Aeronautics and Astronautics

GPS is a direct positioning system with an enormous scope of applicability. Various differential techniques have been used to augment performance in a specific domain. The same signal has been used for continental aircraft guidance (WAAS), local area differential navigation (LAAS), precise aircraft landing navigation, and vehicle attitude determination all with the same fundamental receiver hardware technology. Given this broad scope, we envision a spacecraft, for example, which could sense attitude, absolute orbit position, relative position to nearby spacecraft, angular velocity, and elastic deformation all from the same antennas and receivers. This system could be integrated with other sensors to improve bandwidth or accuracy when necessary.

The highest level of GPS sensor accuracy relies on measurement of the signal's carrier phase. The GPS carrier provides a centimeter level position observable to receivers in continuous track of the carrier. The measurement requires very accurate timing as well as methods of resolving the carrier cycle ambiguity. Techniques for meeting these requirements (such as differencing to remove common mode errors and geometrical cycle ambiguity resolution) have already been demonstrated. The GPS laboratories at Stanford have been working on some specific applications which use the carrier observable:

Past:

- Land and space vehicle attitude determination[3, 4]
- High integrity aircraft landing[5]
- Vehicle angular velocity determination[9]
- Local area autonomous aircraft navigation/control[8]
- Control of autonomous space robots[14]

Current:

- Navigation and control of autonomous farm and construction vehicles[10]
- Tracking and navigation of land vehicles[1]
- Large flexible structure sensing and control[12, 13]
- and several others.

The rest of this paper discusses the latest results of our research on GPS for structural deformation sensing. As previously shown in simulation by Teague[12], differential carrier phase tracking provides a valuable observable for measuring the elastic motions of a structure which exhibits vibrations within the bandwidth and deflection sensitivity limits of available GPS receivers. The observable is the difference in a signal's phase angle as seen by two antennas. By mounting an array of antennas on a flexible body, relative motions may be sensed. A test facility has been constructed at Stanford to evaluate the sensor and to test its applicability for real-time feedback control. This paper focuses on explaining certain important issues which concern this research, and on describing the experimental setup. Experimental data and the results of data processing algorithms are shown and analyzed.

2 GPS Differential Carrier Phase Issues

2.1 Planar Wavefronts

Most of the previous studies of differential carrier phase (DCP) assumed that the received wavefronts were planar. This is a very good assumption for antennas whose baseline length (the distance between antennas) is small relative to the distance to the signal source. Many uses of pseudolites[2], transmitters of GPS-like signals, have been found to enhance or enable GPS sensing systems, but signal wavefronts from pseudolites often cannot be assumed planar.

Pseudolites may be used to provide signals in places where satellite signals are blocked or simply not present, or to enhance measurement accuracy such as:

- in the valleys of mountainous regions
- indoors, for research or for manufacturing
- in deep space, for vehicle relative positioning
- for integer ambiguity resolution in local areas
- for improved signal geometry
- for providing redundant measurements

Non-planar wavefronts introduce two difficulties not present in the planar case. First, the measurement equation is non-linear. This increases the computational load for state estimators. Second, the position of the transmitter phase centers must be known in all three dimensions. For planar waves, only the line-of-sight direction is important.

Fig. 1 shows the geometry of a transmitter, T, and two antennas, A_1 and A_2. As a simplifying assumption, let TA_1A_2 define a *right* triangle. d is the distance from T to A_1, and $d+e$ is the distance from T to A_2. T_r is the actual position of the transmitter, and r denotes a radial uncertainty in that position. If the line of sight is assumed to be along the line from A_1 to T, the DCP would be zero for the planar assumption (the planar DCP is the component of the vector between antennas in the line of sight direction). Thus, the *actual* DCP is the error in this assumption. For $r = 0$, the actual DCP is

$$e = |\underline{p}^{TA_2}| - |\underline{p}^{TA_1}|$$

or,
$$e = d\left(\sqrt{1+(b/d)^2} - 1\right),$$

where $|\underline{p}^{XY}|$ denotes the length of the position vector from point X to point Y. A plot of this equation is shown in Fig. 2 for several baseline lengths, b. For small b/d (the log-linear portion of the plot),

$$e \approx \frac{b^2}{2d}.$$

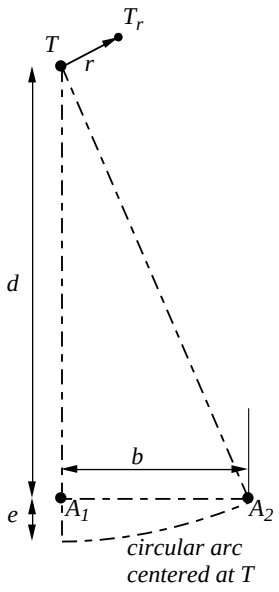

Figure 1: Non-planar waves

Errors in the millimeters are significant for DCP sensing. For our current indoor experiment, the closest pseudolite transmitter is 20 meters away and our baselines are approximately 4 meters. The planar assumption would introduce $\sim$ 40 cm of error, or over two full carrier wavelengths! For our experiment, non-linear measurement equations and the corresponding gradient equations for estimation and control were obtained using the *Autolev* and *Maple* symbolic manipulator packages.

To examine the effect of transmitter position estimate error on DCP error, we compute

$$E_r = \left(|\underline{p}^{TA_2}| - |\underline{p}^{TA_1}|\right) - \left(|\underline{p}^{T_rA_2}| - |\underline{p}^{T_rA_1}|\right)$$

(The first quantity in parentheses is the assumed DCP and the second is the actual.) Fig. 3 shows E_r plotted vs. r, the radial offset, for several values of d. The error is averaged on a circle of radius r. Again, the error falls rapidly as d increases. This shows the importance of good transmitter position estimates when using pseudolites. For our experiment, we will need to know transmitter positions to within a sphere of about 20 cm diameter from truth. Often, the positions can be estimated using the transmitted signal itself through a static self-survey, as is the case in our lab.

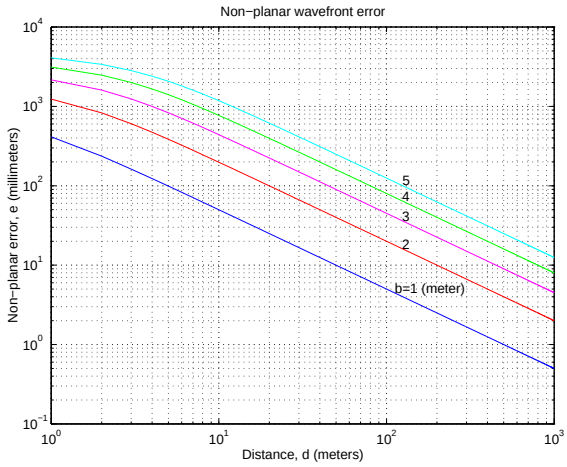

Figure 2: Error due to Planar Wavefront Assumption

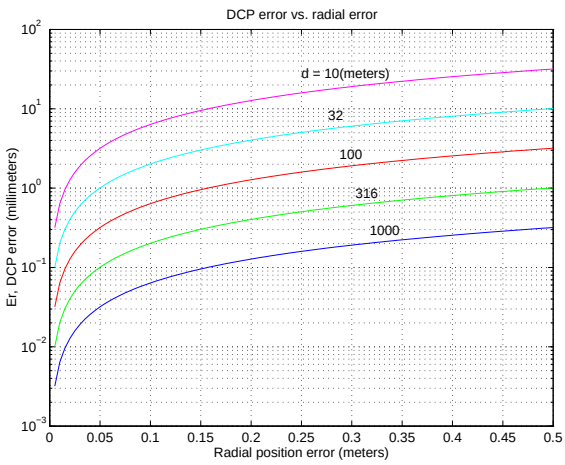

Figure 3: Error due to Transmitter Position Estimate Error

2.2 Antenna/Receiver Arrays and Measurement Synchronization

GPS systems with a large number of antennas are valuable when relative motions of many points on rigid and elastic bodies are important. These relative motions contain information about the deformations and orientations of a body with respect to itself and other bodies. It is sometimes not practical or possible to provide the same time reference to the measurements at each antenna. Some special techniques are required to synchronize the measurements. Fig. 4 shows a generalized configuration of multiple antennas and receivers which we will use to study some different cases.

A_1 through A_5 are antennas and R_1 through R_3 receivers. For now, let a receiver be defined as a unit with a single time reference (clock). The fundamental measurement of differential carrier phase at two antennas requires the same time reference for each antenna, or accurate resolution of the offset between references. Let the DCP between two of the antennas be denoted ϕ_{ij}, where i and j are antenna indices. We will consider three cases:

Time synchronization of measurements on separate receivers

ϕ_{12}, ϕ_{23}, and ϕ_{45} are directly observable at R_1, R_2, and R_3, respectively. But to use these measurements for real-time control, the relative time of applicability of the measurements must be known. The accurate absolute standard GPS time that typically is available in receivers is the result of the four state position fix which uses pseudorange[11] information from four or more satellites. This position fix may not be necessary or available in some DCP systems.

Our lab uses pseudolites which do not broadcast the data needed to resolve pseudorange, and our receivers are not encumbered with pseudorange position fix processing. The simplest method found to time the receiver measurements was to broadcast a simple data message at the standard GPS data rate (50 bits per second, 30 seconds long) from a transmitter in view of antennas from separate receivers, and to synchronize the receivers on the data message arrival (see [14]). This results in a re-synch every 30 seconds. Given the stability and accuracy of standard quartz oscillators, a worst case offset of 3 kHz between the 1.5 GHz receiver oscillators may be assumed. This corresponds to $2\text{x}10^{-6}$ sec/sec of relative clock rate, which adds up to 60 μs over the 30 second data epoch. For our experiment at 20 Hz, this is only 0.12% of the sampling interval. In practice, the divergence will often be much smaller.

DCP between antennas on different receivers with a physical connection

If DCP between A_1 and A_3 is desired (ϕ_{13}), there are a few possibilities:

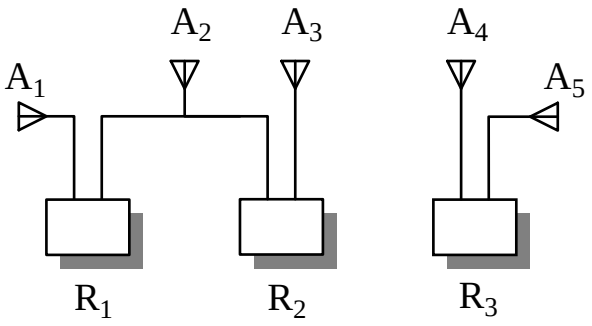

Figure 4: Multiple antennas

1. Add another receiver (or channel in a receiver). This could be the easiest solution.
2. Provide a physical link between receivers R_1 and R_2 to carry the clock signal. Delays and distortion in the link would need to be addressed, and the line bias would need to be calibrated or estimated in real-time.
3. Use the signal at A_2 to synchronize the clocks. Slaving the clocks of R_1 and R_2 to the C/A code phase epoch[11] at A_2 could allow differencing of the phase of a signal visible at A_1 and A_3. Again, a line bias will be present.

DCP between antennas on different receivers with *no* physical connection

The most difficult synchronization task involves differencing phases from separated receivers, such as between A_3 and A_4 on Fig. 4. This occurs when the physical distance between antenna locations is such that an antenna cable is not feasible or convenient, and when antennas reside on completely independent bodies. The latter is the case for rendezvous maneuvers such as mid-air aircraft refueling, and spacecraft docking, for example. Here are three possible techniques:

1. Provide a communication channel between receivers which provides clock corrections. The requirements would put high demands on such a communication link which could be difficult and/or expensive.
2. Use second difference algorithms to eliminate the relative clock error. This technique has been demonstrated by Zimmerman[14] and others.
3. Coherent re-transmission of a satellite signal at a pseudolite location (the "omni-marker" concept) is currently under investigation as a means of eliminating timing errors by Cohen, et. al. at Stanford.

3 A Testbed for Structural Deformation Sensing Using GPS

3.1 Test Structure Physical Characteristics

For testing and development of sensors and controls, a structure has been built which moves in an analogous way to a flexible orbiting space structure. The structure consists of three 60 kg rigid bodies each of which is suspended from above by a twelve meter thread that is attached near the center of mass of the body. This allows 5 DOF movement of the body and minimizes the frequency of suspension induced pendulum modes. Each rigid body consists of a 25 cm cube with two 1.8 meter rigid arms on which sensors are mounted. The suspension thread's point of attachment to the cube can be finely adjusted in three dimensions for balancing using a mechanism which sits at the base of a frustum cut in the top of each cube (see Fig. 6c).

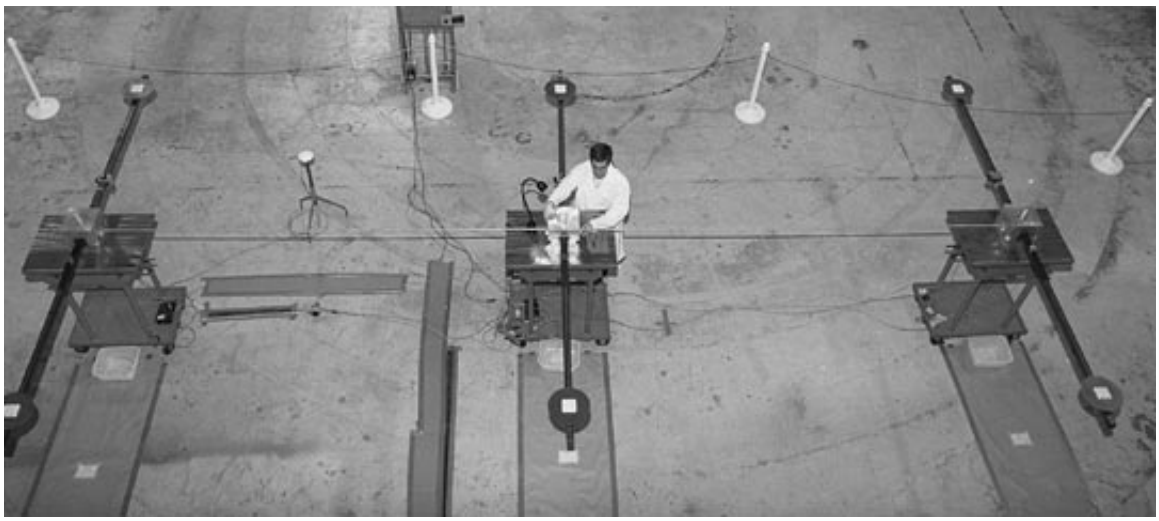

Figure 5: Test Structure

The rigid bodies are connected in a horizontal line with two highly flexible beams of 4 meter long 1/2 inch diameter thin-walled aluminum tubing. The arms of the rigid bodies are perpendicular to this line (see Fig. 5). The combination of massive, center of mass supported rigid bodies, and highly flexible beams results in a system which slowly bends and twists the beams in free motion. The system exhibits many vibration modes below 1 Hz, and arm endpoint (the location of GPS sensors and actuators) deflection magnitudes which are significant relative to the overall structure size. To provide an additional rigid body degree of freedom, the suspension threads are attached at the top to a beam which can rotate freely about a vertical axis. For more details, see [12].

3.2 Sensors and Control Actuators

The structure is outfitted with six Trimble survey-class patch antennas, one at the end of each arm (see Figs. 5 and 6b). The antennas are attached to two Trimble TANS Quadrex© receivers whose core code was modified to provide 20 Hz DCP measurements. Each receiver is connected to three antennas, leaving a free port on each. The free port is being used now for static antennas during testing and development, and can be used to enhance observability in the future, if necessary. The antennas/receivers measure GPS signals broadcast by six custom built signal generators and helical transmit antennas (see Fig. 6d) which are mounted on the walls and ceiling of the large (60x30x20 meters) test room. A helical antenna was chosen to provide a narrow beamwidth signal to minimize multipath interference in the indoor environment. For an independent measure of structural motion, six single-axis Murata Gyrostar© rate gyroscopes are also mounted on the structure (see Fig. 6a). Three gyros are mounted orthogonally on the center body, two on another and only one on another. We will augment the system to the full 9 axes set if in the future, the benefits justify the expense.

A cluster of four on/off cold-gas thrusters is mounted at the end of each arm to provide control actuation (see Fig. 6b). The custom built thrusters produce 1.8 newtons a piece and are turned off and on through a digital output port on the main computer at a maximum frequency of 100 Hz. Actuator location and orientation choice was aided by considering of the energy required to control primary modes of the system using modal controllability grammian analysis.

Our main data processing and control computer is a Pentium PC running a Posix compatible real-time operating system by Lynx Real-Time Systems[7]. GPS data arrives via high-speed serial packet communication. The gyroscopes are read through a PC bus I/O card which also sends control commands to the thrusters. We are currently using and writing "multi-threaded" real-time code in C.

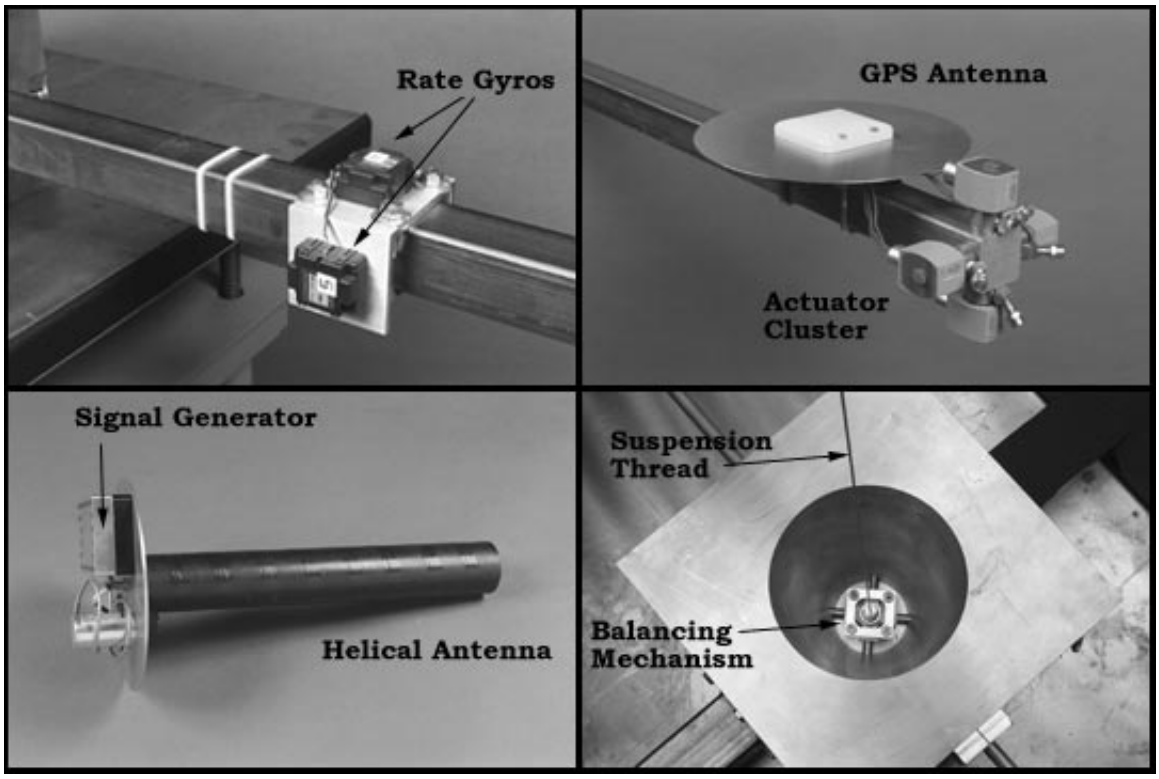

Figure 6: Testbed details. Clockwise from top-left: a. Rate-gyros, b. Actuator cluster and GPS antenna, c. Thread point-of-attachment, d. Transmit antenna

3.3 Data/Results

Data was collected during a series of free-motion tests. Thirty-six DCP and six rate-gyro observables were recorded. The structure was lifted from its support tables, and balanced. First, random excitation was applied which attempted to introduce energy into the four primary system vibration modes. A representative sample of one of the GPS DCP and simultaneous integrated gyroscope readings taken during the subsequent free motion is shown in Fig. 7. The gyroscope curve shown is the integrated angular rate about the horizontal axis perpendicular to the arms of the center body, and the GPS curve shows DCP between the two antennas on the same body. GPS measures rotation about two body fixed axes while the gyro only measures one. This explains the appearance of an additional harmonic component in the GPS curve. The expected phase and frequency agreement is noticeable between the two curves. The power spectra of all the GPS and gyro data for this test are displayed in Fig. 8. The gyro spectrum is divided by frequency to allow one-to-one comparison of rates with positions in the frequency domain. Modal behavior is shown by the clear resonance peaks which agree between the independent GPS and gyroscope sensors. The structural energy observed by GPS is shown to be well above the ambient noise floor of the sensor. Also, the plot illuminates GPS's superior low frequency detection as compared to the rate sensors. GPS detects the very low frequency suspension induced pendulum modes which are invisible to the gyros.

To identify the primary system modes, the researcher attempted to excite individual modes in the structure and collected data. The spectra of each of these four trials is plotted with the randomly excited trial in Fig. 9. This identifies the modes as:

Mode	1^{st} bending	2^{nd} bending	1^{st} twist	2^{nd} twist
Frequency(Hz)	0.145	0.173	0.100	0.168

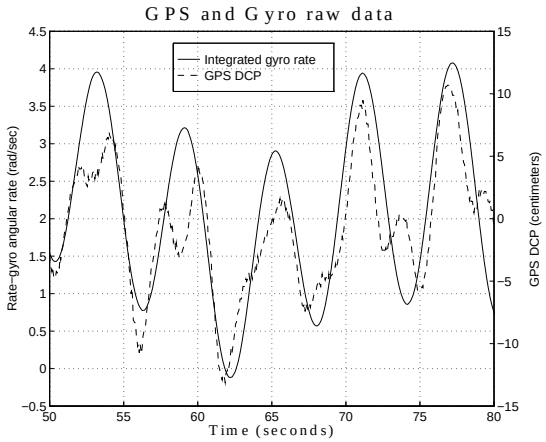

Figure 7: Free vibration data

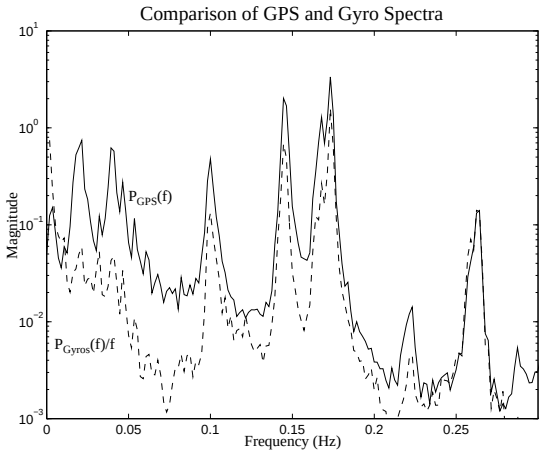

Figure 8: Free motion sensor spectra

The slight misalignment of the first-twist-mode plot is suspected to be due to a repair of the structure between trials. Other peaks in the spectra are due to suspension induced modes.

In our current receivers, a DCP measurement is the difference in phase at a "master" antenna and one of the "slave" antennas. The vector between the antennas is called the "baseline vector." To map phase measurements into the state space, an estimator was developed based on the following measurement equation:

$$\Delta\phi_{ij} = |\underline{p}^{N_j P_i}| - |\underline{p}^{N_j P_M}| - \lambda\eta_{ij} + b_i + \nu_{ij}$$

where,

$\Delta\phi_{ij}$	-	DCP of baseline i, transmitter j
P_i	-	the point corresponding to the phase center of antenna i ($i = M$ denotes the master antenna)
N_j	-	the point corresponding to the phase center of transmit antenna j
$\underline{p}^{N_j P_i}$	-	position vector from N_j to P_i
λ	-	the GPS L_1 carrier wavelength (19.03cm)
η_{ij}	-	the cycle ambiguity, baseline i, transmitter j
b_i	-	the line bias of baseline i
ν_{ij}	-	stochastic noise

For more discussion of the DCP measurement equation, see [6, 12, 14].

As an initial test of the validity of the sensor system and the measurement equation, a kinematic estimation of the simple motion of one of the rigid bodies was performed. From its resting place on its support table, the central body was manually rotated by 5-10 degrees about the flexible beam axis of the structure, and returned to its original position over a period of $\sim$5 seconds. The resulting phase measurements and states are plotted in Fig. 10. The twist angle shows the intended motion and the bend angle exhibits unintentional misalignment of the motion. This test verifies the correctness of the measurement equation as formulated by our symbolic manipulator codes. However, for state estimation including flexible deformations, a dynamic estimator which makes use of a structural dynamic model will be used.

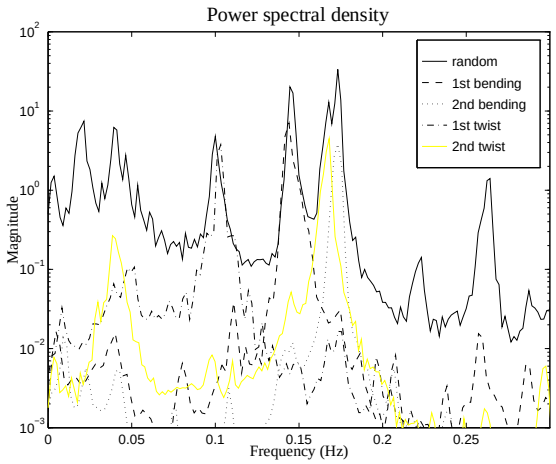

Figure 9: Modal spectrum comparison

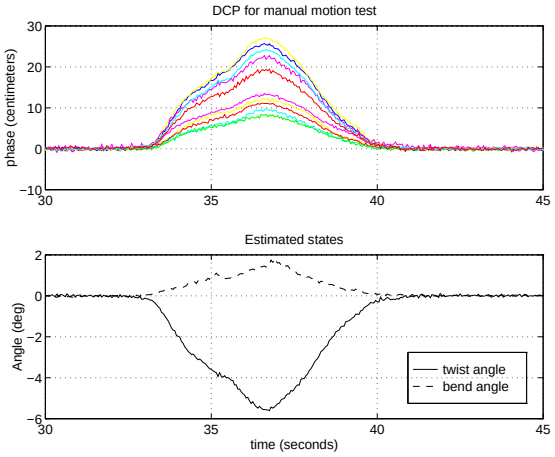

Figure 10: Manual motion phases and angular deflections

4 Conclusions

The DCP error due to a planar wavefront approximation has been shown to be significant for pseudolite applications and the rule-of-thumb, $e \approx \frac{b^2}{2d}$ presented. Also, the error due to imperfect knowledge of transmitter phase center locations for the non-planar case was quantified. Techniques for resolving timing synchronization issues in DCP systems which contain multiple clock references were examined. This is especially important for systems with a large number of antennas, and systems with antennas on independently moving bodes.

These general DCP topics arose before and during our design of an experiment to control elastic structural motion using GPS as the primary motion sensor. We now have a testbed for sensor and control design and for testing, and current data verifies the sensor capability and the hardware setup. A simple kinematic estimator serves as a check on the current measurement equation formulation and data reduction algorithms. These preliminary results are an encouraging foundation for further study. Detailed work on our lab experiment is planned for these areas:

- Structural model refinement and order reduction
- Transmitter phase center self-survey estimation
- Expansion of real-time processing algorithms for cycle ambiguity resolution and dynamic state estimation
- Real-time control

Acknowledgments

The authors wish to acknowledge the generous help from several institutions and individuals who made this research possible. Kurt Zimmerman, Stewart Cobb, and Clark Cohen at Stanford are gratefully acknowledged for their help and insight. We thank the skilled machinists Blaine Bolich and Wolfgang Jung who helped fabricate the test structure. Thanks to Lynx Real-Time Systems for their generous software discounts, and to Trimble Navigation Ltd. who provided the receiver hardware (and access to proprietary source code). This research was funded by NASA.

References

[1] Eric Abbott and David Powell. An Examination of the Relative Merits of Various Sensors for Vehicle Navigation. In *Proceedings of the Institute of Navigation GPS-95 Conference*, Palm Springs CA, September 1995.

[2] H. Stewart Cobb, Clark E. Cohen, and Bradford W. Parkinson. Theory and Design of Pseudolites. In *Proceedings of the Institute of Navigation, National Technical Meeting*, San Diego CA, January 1994.

[3] C. E. Cohen, E. G. Lightsey, B. W. Parkinson, and W. A. Feess. Space Flight Tests of Attitude Determination Using GPS. In *Proceedings of the Institute of Navigation GPS-93 Conference*, Salt Lake City UT, 1993.

[4] C. E. Cohen and B. W. Parkinson. Aircraft Applications of GPS-based Attitude Determination. In *Proceedings of the Institute of Navigation GPS-92 Conference*, Albuquerque NM, 1992.

[5] Clark Cohen, David Lawrence, Boris Pervan, H.Stewart Cobb, Andrew Barrows, David Powell, Bradford W. Parkinson, Victor Wullschleger, and S. Kalinowski. Flight Test Results of Autocoupled Approaches using GPS and Integrity Beacons. In *Proceedings of the Institute of Navigation GPS-94 Conference*, Salt Lake City UT, 1994.

[6] Clark Emerson Cohen. *Attitude Determination Using GPS*. PhD thesis, Stanford University, Department of Aeronautics and Astronautics, Stanford, CA 94305, December 1992.

[7] Lynx Real-Time Systems, 2239 Samaritan Drive, San Jose, CA 95124. *LynxOS 2.3.0 Users Manuals*, 1995.

[8] Paul Y. Montgomery. *Carrier Differential GPS for Automatic Control*. PhD thesis, Stanford University, Department of Aeronautics and Astronautics, Stanford, CA 94305, (to be published) June 1996.

[9] Paul Y. Montgomery, H. Uematsu, and B. W. Parkinson. Analysis of Angular Velocity Determination Using GPS. In *Proceedings of the Institute of Navigation GPS-94 Conference*, Salt Lake City UT, 1994.

[10] Michael L. O'Connor, Gabriel H. Elkaim, and Bradford W. Parkinson. Kinematic GPS for Closed Loop Control of Farm and Construction Vehicles. In *Proceedings of the Institute of Navigation GPS-95 Conference*, Palm Springs CA, September 1995.

[11] Bradford W. Parkinson, James J. Spilker, Penina Axelrad, and Per Enge. *GPS: Theory and Applications*. American Institute of Aeronautics and Astronautics, Washington, DC, 1996.

[12] E. Harrison Teague, Jonathan P. How, London G. Lawson, and Bradford W. Parkinson. GPS as a Structural Deformation Sensor. In *Proceedings of the AIAA Guidance, Navigation and Control Conference*, Baltimore MD, August 1995.

[13] E. Harrison Teague and Bradford W. Parkinson. *Translation, Rotation, And Vibration Control of Large Space Structures Using Self-Differential GPS (SDGPS)*, volume 81 of *Guidance and Control*, chapter 1, pages 93–101. American Astronautical Society, 1993.

[14] K. R. Zimmerman and R. H. Cannon Jr. GPS-Based Control for Space Vehicle Rendezvous. In *Proceedings of the Institute of Navigation GPS-94 Conference*, Salt Lake City UT, September 1994.